

Theory of helical spin crystals: Phases, textures, and properties

B. Binz* and A. Vishwanath

Department of Physics, University of California, 366 Le Conte # 7300, Berkeley, California 94720-7300, USA

(Received 4 August 2006; published 11 December 2006)

Motivated by recent experiments on the itinerant helimagnet MnSi, we study general properties of helical spin crystals -magnetic structures obtained by superposing distinct spin spirals. An effective Landau description of helical spin crystals is introduced and simple rules for stabilizing various spin crystal structures over single spirals are established. Curious properties of the magnetic structures so obtained, such as symmetry stabilized topological textures and missing Bragg reflections are pointed out. The response of helical spin crystals to crystalline anisotropy, magnetic field and nonmagnetic disorder are studied, with special reference to the bcc1 spin structure, a promising starting point for discussing the partial order phases seen at high pressure in MnSi. Similar approaches may be applied to other crystallization problems such as Larkin-Ovchinnikov-Fulde-Ferrel states in spin-imbalanced superconductors.

DOI: [10.1103/PhysRevB.74.214408](https://doi.org/10.1103/PhysRevB.74.214408)

PACS number(s): 75.10.-b, 75.30.Kz, 75.90.+w

I. INTRODUCTION

Long period helical spin-order resulting from Dzyaloshinskii-Moriya (DM) spin-orbit coupling¹ in noncentrosymmetric itinerant magnets (e.g., MnSi, Fe_xCo_{1-x}Si, FeGe with crystal structure B20) has been intensively studied in the past.²⁻¹⁰ One material of this family, MnSi, has attracted recent interest because of its puzzling behavior under applied hydrostatic pressure.^{11,12} A state with non-Fermi liquid transport properties¹³ is obtained over a wide range of pressures above a critical threshold p_c . Beginning at the same critical pressure, but over a smaller pressure range, magnetic partial order is observed in neutron scattering experiments.^{14,15} While usual helical order gives rise to sharp Bragg peaks in neutron scattering (corresponding to the periodicity of the helical spin-density wave), partial order is characterized by a neutron scattering signal which is smeared over a wave vector sphere rather than localized at discrete points in reciprocal space.

Recent theoretical work on electronic properties, critical fluctuations and collective modes of helimagnets are in Refs. 16–18. Theoretical proposals for the high pressure state of MnSi have invoked proximity to a quantum multicritical point¹⁹ or magnetic liquid-gas transitions.²⁰ Closest in spirit to our approach are the skyrmionlike magnetic patterns studied in Refs. 21 and 22.

Recently, we have proposed a kind of magnetic order, the helical spin crystal, as a promising starting point for a theory of partial order.²³ Helical spin crystals are magnetic patterns, which are obtained by superposition of several helical spin-density waves which propagate in different directions. There is a substantial resemblance to multi- k magnetic structures (also known as multiple q or multiple spin density wave states).^{24–28} But in contrast to most other magnetic multi- k systems, in helical spin crystals the ordering wave vectors are selected from an infinite number of degenerate modes lying on a sphere in reciprocal space—a process analogous to the crystallization of liquids.

In this work, we present a detailed theory of such structures. The stability, structure and distinctive properties of such states are described, and the consequences of coupling to nonmagnetic disorder is discussed.

The paper is organized as follows. First, we review the standard theory of helimagnetism in Sec. II, finishing with a short remark about more general helical magnetic states. Then, the theory of helical spin crystals is developed. The requirements to energetically stabilize helical spin crystal states are investigated in Sec. III. The analysis works in two directions. First, we establish a phase diagram in terms of natural parameters which tune the interaction between helical modes and second, we give simple rules to construct model interactions which stabilize a large class of helical spin crystals. The remaining parts of the paper are dedicated to extracting testable consequences of these magnetic states. In Sec. IV, we give a description of the most prominent spin crystals which emerge from our energetic analysis in terms of their symmetry. It is shown that the symmetry of the magnetic state may stabilize topological textures like merons and antivortices which are otherwise not expected to be stable in the present context, given the order parameter and dimensionality of the system. Symmetry also determines, which higher-harmonics Bragg peaks these structures would produce. We subsequently study the response of helical spin crystals with respect to different perturbations in Sec. V. For example, subleading spin-orbit coupling (crystal anisotropy) locks the magnetic crystal to the underlying atomic lattice and thus determines the location of magnetic Bragg peaks. We also study the response to an external magnetic field which, apart from producing a uniform magnetic moment, also leads to distinctive distortions of the helical magnetic structure, which could be observable by neutron scattering. Finally, in Sec. VI we investigate the implications of nonmagnetic impurities, which are expected to destroy long-range magnetic order and produce diffuse scattering.

II. LANDAU-GINZBURG THEORY OF HELIMAGNETISM

For a cubic magnet without a center of inversion, the Landau-Ginzburg free energy to quadratic order in the magnetization $\mathbf{M}(\mathbf{r})$ is

$$F_2 = \langle r_0 \mathbf{M}^2 + J(\partial_\alpha M_\beta)(\partial_\alpha M_\beta) + 2DM \cdot (\nabla \times \mathbf{M}) \rangle, \quad (1)$$

where $\langle \dots \rangle$ indicates sample averaging, r_0, J, D are parameters ($J > 0$) and Einstein summation is understood. The last

term of Eq. (1) is the DM interaction, which is odd under spatial inversion and originates in spin-orbit coupling.¹ Fourier transformation, $\mathbf{M}(\mathbf{r}) = \sum_{\mathbf{q}} \mathbf{m}_{\mathbf{q}} e^{i\mathbf{q}\cdot\mathbf{r}}$ with $\mathbf{m}_{-\mathbf{q}} = \mathbf{m}_{\mathbf{q}}^*$, leads to

$$F_2 = \sum_{\mathbf{q}} [(r_0 + Jq^2)|\mathbf{m}_{\mathbf{q}}|^2 + 2D\mathbf{m}_{\mathbf{q}}^* \cdot (i\mathbf{q} \times \mathbf{m}_{\mathbf{q}})]. \quad (2)$$

Clearly, the energy is minimal for circularly polarized spiral modes, where $\nabla \times \mathbf{M}$ points in the direction of $-D\mathbf{M}$. For such modes,

$$F_2 = \sum_{\mathbf{q}} r(q)|\mathbf{m}_{\mathbf{q}}|^2, \quad (3)$$

where $r(q) = r_0 - JQ^2 + J(q - Q)^2$ with $Q = |D|/J$. The Gaussian theory thus determines both the chirality of low-energy helical modes and their wavelength $\lambda = 2\pi/Q$. The latter is typically long (between 180 Å in MnSi and 2300 Å in Fe_{0.3}Co_{0.7}Si), reflecting the smallness of spin-orbit coupling effects compared to exchange. However, no preferred spiraling direction is selected by Eq. (1), since F_2 is rotation invariant. Cubic anisotropy terms which break this invariance are of higher order in the spin-orbit interaction and therefore small. We neglect them for the moment and reintroduce them later.

The isotropic Gaussian theory leaves us with an infinite number of modes which become soft as $r(Q) \rightarrow 0$. They consist of helical spin-density waves with given chirality (determined by the sign of D), whose wave vectors lie on a sphere $|\mathbf{q}| = Q$ in reciprocal space. Each of these helical modes is determined by an amplitude and a phase. Hence, for each point \mathbf{q} on the sphere, we define a complex order parameter $\psi_{\mathbf{q}}$ (with $\psi_{-\mathbf{q}} = \psi_{\mathbf{q}}^*$) through

$$\mathbf{m}_{\mathbf{q}} = \frac{1}{2} \psi_{\mathbf{q}} (\hat{\epsilon}'_{\mathbf{q}} + i\hat{\epsilon}''_{\mathbf{q}}), \quad (4)$$

where $\hat{\epsilon}'_{\mathbf{q}}$, $\hat{\epsilon}''_{\mathbf{q}}$, and $\hat{\mathbf{q}}$, are mutually orthogonal unit vectors (with a defined handedness, given by the sign of D). Obviously, changing the phase of $\psi_{\mathbf{q}}$ is equivalent to rotating $\hat{\epsilon}'_{\mathbf{q}}$ and $\hat{\epsilon}''_{\mathbf{q}}$ around $\hat{\mathbf{q}}$. The phase of $\psi_{\mathbf{q}}$ is thus only defined relative to some initial choice of $\hat{\epsilon}'_{\mathbf{q}}$. The neutron scattering intensity is proportional to $|\hat{\mathbf{q}} \times \mathbf{m}_{\mathbf{q}}|^2 = 1/2 |\psi_{\mathbf{q}}|^2$, independent of the phase. Changing the phase of $\psi_{\mathbf{q}}$ is also equivalent to translating $\mathbf{M}(\mathbf{r})$ along $\hat{\mathbf{q}}$.

In the following, we study minima of the free energy in the ordered phase [$r(Q) < 0$]. These depend on the interactions between degenerate modes (i.e., free energy contributions, which are quartic or higher order in \mathbf{M}). We only consider interactions which, as F_2 , have full rotation symmetry and we will include the weak crystal anisotropy last. The most general quartic term which has full rotation symmetry (transforming space and spin together) is of the form

$$F_4 = \sum_{\mathbf{q}_1, \mathbf{q}_2, \mathbf{q}_3} U(\mathbf{q}_1, \mathbf{q}_2, \mathbf{q}_3) (\mathbf{m}_{\mathbf{q}_1} \cdot \mathbf{m}_{\mathbf{q}_2}) (\mathbf{m}_{\mathbf{q}_3} \cdot \mathbf{m}_{\mathbf{q}_4}), \quad (5)$$

with $\mathbf{q}_4 = -(\mathbf{q}_1 + \mathbf{q}_2 + \mathbf{q}_3)$.

A. Single-spiral state

For example, if $U(\mathbf{q}_1, \mathbf{q}_2, \mathbf{q}_3)$ is a constant, then $F_4 \propto \langle \mathbf{M}^4 \rangle$. If the interaction depends only on the local magne-

tization amplitude, i.e., in general if $F = F_2 + \langle f(\mathbf{M}^2) \rangle$ for some function f , then the absolute minimum of F is given by a single-spiral state (also known as helical spin density wave) $\mathbf{M}(\mathbf{r}) = \mathbf{m}_{\mathbf{k}} e^{i\mathbf{k}\cdot\mathbf{r}} + \mathbf{m}_{\mathbf{k}}^* e^{-i\mathbf{k}\cdot\mathbf{r}}$, where a single pair of opposite momenta $\pm \mathbf{k}$ is selected. To prove this, we write F as

$$\sum_{\mathbf{q}} [r(q) - r(Q)] |\mathbf{m}_{\mathbf{q}}|^2 + \langle r(Q) \mathbf{M}^2 + f(\mathbf{M}^2) \rangle. \quad (6)$$

In the single-spiral state, \mathbf{M}^2 is constant in space and it minimizes the first and the second term of Eq. (6) independently. Therefore, no other magnetic state can be lower in energy.

Because Q is small, the relevant wave vectors entering Eq. (5) are also small and $U(\mathbf{q}_1, \mathbf{q}_2, \mathbf{q}_3)$ is effectively close to a constant. Therefore, the single-spiral state, as observed in Fe_xCo_{1-x}Si, FeGe and in MnSi at ambient pressure, is the most natural helical magnetic order from the point of view of Landau theory.

B. Linear superpositions of single-spiral states

Motivated by the phenomenology of partial order, we will now extend the theory beyond this standard solution. We speculate that $U(\mathbf{q}_1, \mathbf{q}_2, \mathbf{q}_3)$ is not constant, such that F_4 favors a linear superposition of multiple spin-spirals with different wave vectors on the sphere of degenerate modes $|\mathbf{q}| = Q$.

One may first speculate about magnetic patterns whose Fourier transform is nonzero everywhere on the wave-vector sphere and peaked infinitely sharply perpendicular to the sphere, i.e.,

$$|\psi_{\mathbf{q}}|^2 \propto \delta(|\mathbf{q}| - Q) \quad (7)$$

[see Eq. (4)]. This idea turns out to be complicated for at least two reasons.

The first complication is that there is no continuous way of attributing a finite-amplitude spiral mode to each point on the wave vector sphere. This can be seen by noting that $\hat{\epsilon}'_{\mathbf{q}}$ [Eq. (4)] is a tangent vector field on the sphere. Thus, it cannot be continuous (impossibility of combing a hedgehog).²⁹ Thus there is no “uniform” superposition of helical modes on the sphere. The problem of singularities can be avoided if one assumes a $\psi_{\mathbf{q}}$ with point nodes on the sphere.

The second complication is that higher harmonics would result in a broadening of the delta function in Eq. (7). This is seen as follows. Consider three momenta $\mathbf{q}_1, \mathbf{q}_2, \mathbf{q}_3$ on the wave vector sphere and \mathbf{q}_4 which is off the sphere. The non-vanishing modes $\mathbf{m}_{\mathbf{q}_1}, \mathbf{m}_{\mathbf{q}_2}, \mathbf{m}_{\mathbf{q}_3}$ couple linearly to $\mathbf{m}_{\mathbf{q}_4}$ via Eq. (5) and thus induce a higher harmonic “off-shell” mode $\mathbf{m}_{\mathbf{q}_4} \neq 0$. Since this happens for every point away from the sphere, the effect is an intrinsic broadening of the peak in $|\psi_{\mathbf{q}}|^2$, in contradiction with the initial assumption of Eq. (7).

III. ENERGETICS OF HELICAL SPIN CRYSTALS

In the following, we study magnetic structures which are superpositions of a *finite* number of degenerate helical modes ψ_j with wave vectors $\pm \mathbf{k}_j$, $j = 1, \dots, N$. We call the resulting states helical spin crystals, because of the analogy

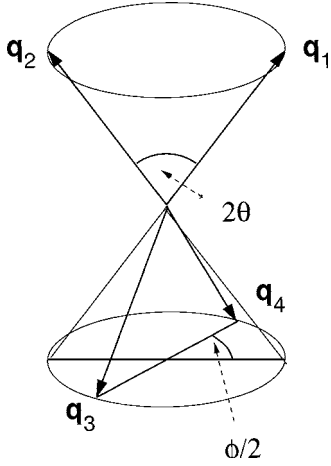


FIG. 1. The set of quartets $(\mathbf{q}_1, \dots, \mathbf{q}_4)$ satisfying $|\mathbf{q}_i|=Q$ and $\mathbf{q}_1+\dots+\mathbf{q}_4=0$, modulo global rotations, may be parametrized by two angles θ and ϕ as shown in this figure.

with weak crystallization theory of the solid-liquid transition.³⁰

A. Structure of the quartic interaction

We assume that F_4 is small, and that its main effect is to provide an interaction between the modes which are degenerate under F_2 . Thus, the relevant terms of F_4 are those with $|\mathbf{q}_1|=|\mathbf{q}_2|=|\mathbf{q}_3|=|\mathbf{q}_4|=Q$. This phase-space constraint and rotational symmetry implies that the coupling function U depends only on two relative angles between the momenta

$$U(\mathbf{q}_1, \mathbf{q}_2, \mathbf{q}_3)|_{|\mathbf{q}_i|=Q} = U(\theta, \phi), \quad (8)$$

where we have chosen the following parametrization:

$$\begin{aligned} 2\theta &= \arccos(\hat{\mathbf{q}}_1 \cdot \hat{\mathbf{q}}_2), \\ \phi/2 &= \arccos\left(\frac{(\hat{\mathbf{q}}_2 - \hat{\mathbf{q}}_1) \cdot \hat{\mathbf{q}}_3}{1 - \hat{\mathbf{q}}_1 \cdot \hat{\mathbf{q}}_2}\right). \end{aligned} \quad (9)$$

Geometrically, $\phi/2$ is the angle between the two planes spanned by $(\mathbf{q}_1, \mathbf{q}_2)$ and $(\mathbf{q}_3, \mathbf{q}_4)$ (Fig. 1). In the special case $\mathbf{q}_1+\mathbf{q}_2=0$, it becomes the angle between \mathbf{q}_2 and \mathbf{q}_3 . This mapping allows θ and ϕ to be interpreted as the polar and azimuthal angles of a sphere and the coupling $U(\theta, \phi)$ is a function on that sphere. Since it describes an effective coupling between modes on the wave vector sphere, the coupling $U(\theta, \phi)$ has a status similar to that of Fermi liquid parameters in the theory of metals.

The Landau free energy $F=F_2+F_4$ of helical spin crystal states is calculated as follows. Obviously,

$$F_2 = r(Q) \sum_j |\psi_j|^2. \quad (10)$$

The quartic term, Eq. (5), may be split into three distinct contributions $F_4=F_s+F_p+F_{nt}$. The first term, F_s , is the self-interaction of each spiral mode with itself,

$$F_s = U_s \sum_j |\psi_j|^4, \quad (11)$$

where $U_s=U(\theta=\pi/2, \phi=0)$. A minimum requirement for stability of the theory is $U_s>0$.

The next term, F_p , stems from pairwise interactions between modes. It is of the form

$$F_p = 2 \sum_{i<j} V_p(\theta_{ij}) |\psi_i|^2 |\psi_j|^2, \quad (12)$$

where $2\theta_{ij}=\arccos(\hat{\mathbf{k}}_i \cdot \hat{\mathbf{k}}_j)$ and

$$V_p(\theta) = U\left(\frac{\pi}{2}, 4\theta\right) + \sin^4 \theta U(\theta, 0) + \cos^4 \theta U\left(\frac{\pi}{2} - \theta, 0\right). \quad (13)$$

Since $\lim_{\theta \rightarrow 0} V_p(\theta)=2U_s$ is large and positive, F_p provides an efficient repulsion of modes which are too close on the wave vector sphere. Energetically stable superpositions of spirals require substantially smaller values of $V_p(\theta)$ and therefore big-enough angles between them (Sec. III C). This “mode repulsion” suggests that a continuous distribution of Fourier modes on the wave vector sphere, as discussed in Sec. II B, is difficult to stabilize energetically by slowly varying coupling functions $U(\theta, \phi)$. However, singular behavior of the coupling function is conceivable when discussing effective interactions of low energy modes.³¹

Finally, the nontrivial quartic term F_{nt} stems from quartets of modes, whose wave vectors sum up to zero. The geometry of four equal-length wave vectors summing to zero is depicted in Fig. 1. A quartet-contribution occurs for $0<2\theta<\pi$ and $0<\phi/2<\pi$. In this case, the eight wave vectors $\pm\mathbf{k}_j$ form the vertices of a cuboid. Hence,

$$F_{nt} = \sum'_{j_1<\dots<j_4} F_{j_1 j_2 j_3 j_4}, \quad (14)$$

where the summation is over such quartets. For example, if $\mathbf{k}_{j_1}+\mathbf{k}_{j_2}+\mathbf{k}_{j_3}+\mathbf{k}_{j_4}=0$, there is a term $F_{j_1 j_2 j_3 j_4} \propto \psi_{j_1} \psi_{j_2} \psi_{j_3} \psi_{j_4}$. The algebra of these terms, which depend on the relative phases of modes, is rather lengthy and obviously depending on the phase convention used to define the ψ variables.

The term F_{nt} fixes the relative phases of ψ_j to minimize the energy. If there is no frustration between minimizing each individual quartet term, the phases arrange in such a way that all $F_{j_1 j_2 j_3 j_4} \leq 0$. It follows that $F_{nt} \leq 0$, after minimization for the ψ phases. A special case is the quartet of modes, whose wave vectors $\pm\mathbf{k}_j$ form the vertices of a cube (e.g., modes along $\langle 111 \rangle$). In this case, $F_{j_1 j_2 j_3 j_4}=0$ independently of the coupling function $U(\theta, \phi)$ as a consequence of rotational symmetries.³² This is the reason why no such quartet term appears in the theory of Bak and Jensen.⁶ As a consequence, a superposition of four modes along all $\langle 111 \rangle$ directions is necessarily unstable towards shifting the wave vectors away from the perfect cubic configuration in order to gain energy from F_{nt} (see description of fcc* below).

B. Phase diagram

If $U(\theta, \phi)$ is only slowly varying, it is justified to expand it in spherical harmonics (Y_{lm}). That is,

$$U(\theta, \phi) = U_0 + U_{11} \sin \theta \cos \phi + U_{20}(3 \cos^2 \theta - 1) + U_{22} \sin^2 \theta \cos 2\phi, \quad (15)$$

where we retained all terms with $l \leq 2$, which satisfy the relation $U(\theta, \phi) = U(\pi - \theta, \phi) = U(\theta, 2\pi - \phi)$.

Different quartic expressions in terms of the real-space magnetization $\mathbf{M}(\mathbf{r})$ may lead to the same projected coupling $U(\theta, \phi)$. For example, the three terms

$$\langle W\mathbf{M}^4 + W'[\nabla(\mathbf{M}^2)]^2 + W''(\partial_\alpha M_\beta)(\partial_\alpha M_\beta)\mathbf{M}^2 \rangle \quad (16)$$

lead to $U(\mathbf{q}_1, \mathbf{q}_2, \mathbf{q}_3) = W + W'(\mathbf{q}_1 + \mathbf{q}_2)^2 - W''\mathbf{q}_1 \cdot \mathbf{q}_2$. When projected onto the wave vector sphere, they generate only two spherical harmonics, namely

$$U_0 = W + \frac{1}{3}(4W' + W'')Q^2, \\ U_{20} = \frac{2}{3}(2W' - W'')Q^2. \quad (17)$$

The terms W and W' have intuitive interpretations: W restricts the magnetization amplitude, whereas W' favors or disfavors modulations of \mathbf{M}^2 , depending on the sign.³³ In the following, we set $W''=0$ and use the four parameters W , W' , U_{11} , and U_{22} to tune the interaction $U(\theta, \phi)$.

It is hard to find the exact global minimum of $F_2 + F_4$ for a general coupling function $U(\theta, \phi)$. We therefore restrict ourselves to a certain variational class of magnetic states and determine the minimum within this class. Recently,²³ we studied only states which can be obtained by superposition of those six modes which propagate along the $\langle 110 \rangle$ directions (six-mode model). Here, we explore a much broader class of states. We include

(1) any superposition of those 13 spin-spirals which propagate along the directions³⁴ $\langle 111 \rangle$, $\langle 110 \rangle$, and $\langle 100 \rangle$ (13 complex variables ψ_j as variational parameters),

(2) any superposition of up to four spirals with arbitrary propagation direction (four variables ψ_j and five independent angles between wave vectors as variational parameters).

Within these constraints, we have computed³⁵ a phase diagram as a function of the coupling parameters W , W' , U_{11} , and U_{22} , shown in Figs. 2 and 3.

All magnetic ground states are equal-amplitude superpositions of 1, 2, 3, 4 or 6 spiral modes. The body-centered-cubic (bcc) states are superpositions of all $\langle 110 \rangle$ modes. bcc1 and bcc2 differ by the relative phases of the six interfering helical modes (see Sec. IV A 1). The simple cubic (sc) crystal consists of three mutually orthogonal spirals (e.g. along all $\langle 100 \rangle$ directions). A face-centered-cubic (fcc) helical spin crystal is obtained by superposing all four $\langle 111 \rangle$ modes. However, the ground state is not fcc but a small distortion of it, fcc^* . In fcc^* , the wave vectors are shifted slightly away from $\langle 111 \rangle$ in order to gain energy from the quartet-term F_{nt} .³⁶ The symbols “ Δ ” and “ \square ” are used differently here than in our previous paper.²³ Here, “ \square ” stands for a superposition of four modes with wave vectors as shown in Fig. 1 with $\phi/2 = \pi/2$. Hence, wave vectors $\pm \mathbf{k}_j$ form a square cuboid and allow for one quartet term F_{nt} . The angle 2θ changes as a function of interaction parameters within the range $0.24\pi < 2\theta < 0.38\pi$. Finally, the phase “ Δ ” consists of three modes. The wave vectors $\mathbf{k}_1, \mathbf{k}_2, \mathbf{k}_3$ point to the vertices of

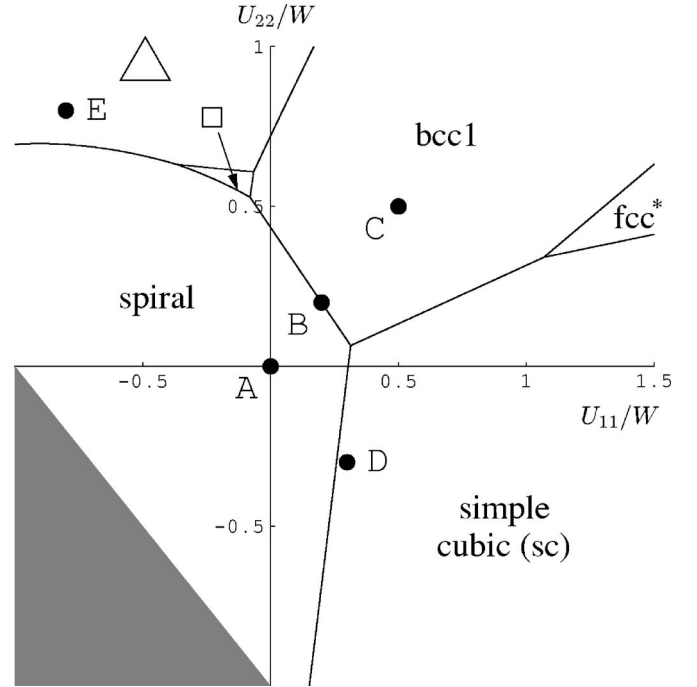


FIG. 2. Phase diagram for $W > 0$ and $W' = 0$. In the gray region, $F_4 < 0$ and the quartic theory is unstable. The various phases are explained in the text. In contrast to our earlier use of these symbols (Ref. 23), “ Δ ” and “ \square ” denote general states with 3 and 4 helical modes, respectively.

an equilateral triangle on the sphere, whose size is determined by the requirement that the mutual angle between two wave vectors, 2θ , minimizes Eq. (13). The angle 2θ is parameter dependent and lies in the range $0.14\pi < 2\theta < 0.24\pi$.

As expected, a negative W' [Eq. (16)] favors multimode spin crystal states with varying magnetization amplitude relative to the spiral state with constant \mathbf{M}^2 (compare Figs. 2 and 3). Positive W' has the opposite effect, and enhances the region of the spiral phase (not shown). The term W' alone (i.e., with $U_{11} = U_{22} = 0$) stabilizes sc in the regime $Q^2 W' < -W/2 < 0$. However, a small positive U_{22} is sufficient to favor bcc1 over sc.

In conclusion, we observe that two helical spin crystals, bcc1 and sc, appear adjacent to the single-spiral state and are stable at relatively small values of $Q^2 W'$, U_{11} , and U_{22} . In the following, we study the properties of the bcc1, and sc states since they are the most likely candidates of helical spin crystals from the point of view of energetics.

C. Model interactions with exact ground states

In the preceding section, we established a variational phase diagram for “natural,” i.e., slowly varying coupling functions $U(\theta, \phi)$. Most phases in this phase diagram (“spiral”, sc, bcc1, bcc2, fcc, and “ Δ ”) can be shown to be the *exact* global minima for some fine-tuned model interaction, that are constructed below.

Let us consider the toy model $F_{\text{toy}} = F_2 + F_s + F_p$ [Eqs. (10)–(12)] where the quartet term F_{nt} is dropped and we replace $V_p(\theta)$ by a constant V . In this model, local minima

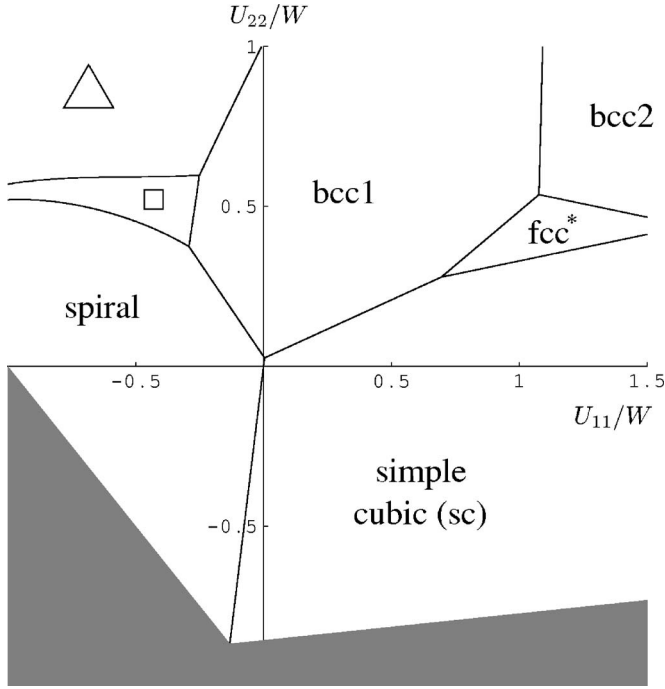


FIG. 3. Same as Fig. 2 with $Q^2W' = -0.5W$. The point $U_{11} = U_{22} = 0$ is now at the phase boundary between spiral order and simple cubic.

with N nonvanishing modes ($N \geq 1$) must have equal amplitudes $|\psi_j|^2 = |r|/(U_s - V + NV)/2$ and the minimum energy with N modes is

$$F_{\text{toy},N} = -\frac{1}{4} \frac{r^2}{V + \frac{U_s - V}{N}}. \quad (18)$$

There are three regimes. If $0 < U_s < V$, the ground state is the single-mode phase with $N=1$ (all but one ψ are zero). For $0 < V < U_s$, the energy is monotonically decreasing with N . It means that the system includes as many modes as possible to lower its energy. Finally, for $V < 0$ or $U_s < 0$, F_{toy} is not bounded from below and therefore unstable.

To make use of this toy model, we must tune the interaction such that $U(\theta, \phi) \rightarrow 0$ unless $\theta = \pi/2$ or $\phi = 0$. This removes the quartet term F_{nt} and we are left with a model similar to F_{toy} with the difference that $V_p(\theta)$ is not constant.

We now tune the interaction such that $V_p(\theta)$ is very big³⁷ everywhere except at some angle θ_{opt} , where it has a narrow minimum. For such a pair interaction, all arrangements of modes which involve angles other than $2\theta_{\text{opt}}$ are excluded. Within this constraint, we are left with our toy model with a constant pair interaction $V = V_p(\theta_{\text{opt}})$, but the number of modes is restricted to $1 \leq N \leq 3$, since no more than three modes can have equal mutual angles between them. It is clear that in the region $-3U_s/2 < V_p(\theta_{\text{opt}}) < U_s$, the ground state is a helical spin crystal with three modes, i.e., the state “ Δ ” or sc (in the case $2\theta_{\text{opt}} = \pi/2$).

A different class of exact ground states is obtained, if the interaction is tuned such that

- (1) $V_p(\theta)$ is very big³⁷ in the region $0 < 2\theta < 2\theta_c$ and

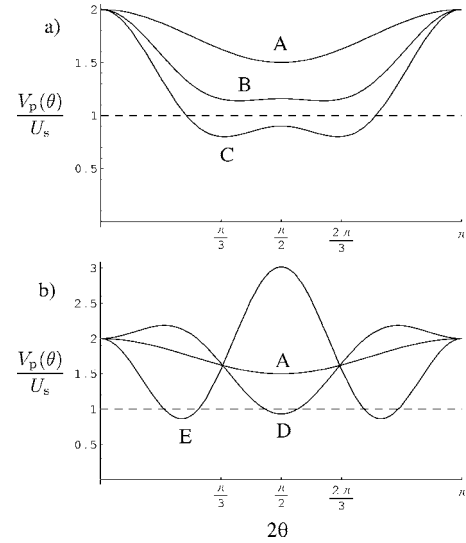


FIG. 4. (a) and (b) For the locations A, \dots, E in the phase diagram of Fig. 2, the ratio between the pair interaction $V_p(\theta)$ and the self-interaction U_s is plotted as a function of the angle 2θ (the angle between propagation directions of modes). A , single-spiral state; B , phase boundary between single-spiral and bcc1; C , bcc1; D , sc; E , Δ .

- (2) $V_p(\theta) = V$ (constant) in the region $2\theta_c \leq 2\theta \leq \pi/2$ for some critical angle $2\theta_c$. In this way, modes whose wave vectors are too close are excluded. That is, it enforces a “hard sphere” constraint $|\hat{\mathbf{k}}_i \pm \hat{\mathbf{k}}_j| \geq 2(1 - \cos 2\theta_c)$ on the wave vectors. The interaction between modes which satisfy this constraint is constant and reduces to the toy model. Therefore, if $V < U_s$ the ground state will include as many modes as geometrically possible by the “hard sphere” constraint. In the case $2\theta_c = \arccos 1/3$, we obtain fcc, which has wave vectors at the vertices of a cube. In the case $2\theta_c = \pi/3$, we obtain bcc whose wave vectors are the vertices of a cuboctahedron. This can be seen as follows. A real-space bcc lattice corresponds to a fcc reciprocal lattice and the wave vectors $\pm k_j$ of the bcc spin crystals are the 12 nearest neighbors of the origin in the fcc reciprocal lattice. Because fcc is the cubic close packing of spheres, this represents the only arrangement of 12 vectors $|\mathbf{k}_j| = Q$ which satisfies the constraint $|\hat{\mathbf{k}}_i - \hat{\mathbf{k}}_j| \geq 1$. (The hexagonal close packing is not acceptable because it does not consist of pairs $\pm \mathbf{k}_j$.) In principle, this construction can be used to create models whose ground state contains an arbitrarily high number of modes.

We can now use the insight from these constructed models to understand certain features of the phase diagram of Figs. 2 and 3. In Fig. 4, we plot $V_p(\theta)$ as obtained from the expansion Eq. (15) at different places in the phase diagram of Fig. 2. In the bcc1 region of the phase diagram (curve C), $V_p(\theta)$ is similar to the one constructed above: close to constant and small for $\pi/3 \leq 2\theta \leq \pi/2$, big for $2\theta < \pi/3$. At the phase boundary between single-spiral and bcc1 (curve B), V_p is still bigger than U_s , indicating that the quartet term F_{nt} is essential to stabilize bcc1 close to the phase boundary. The phase boundaries between single-spiral and three-mode states (sc or Δ) are exactly determined by the crossing of the minimum of $V_p(\theta)$ with U_s , as illustrated by curves D and E .

IV. STRUCTURE OF HELICAL SPIN CRYSTALS

A. Symmetry properties and topology of helical spin crystals

Time-reversal symmetry (\mathcal{T}) reverses the magnetization direction $\mathbf{M} \rightarrow -\mathbf{M}$ and may be implemented in terms of the ψ variables as $\psi_j \rightarrow -\psi_j$.

Under spatial translation by a vector \mathbf{a} , the ψ variables transform as $\psi_j' = \psi_j \exp(i\mathbf{k}_j \cdot \mathbf{a})$, i.e., they experience a phase change.

If the set of vectors \mathbf{k}_j is linearly independent, every phase change of modes simply amounts to a global translation. This is the case in helical spin crystals with up to three nonplanar modes, e.g., in sc and Δ . These states are periodic with Bravais vectors $\mathbf{a}_1, \mathbf{a}_2, \mathbf{a}_3$, which are determined by $\mathbf{a}_i \cdot \mathbf{k}_j = 2\pi\delta_{ij}$. It follows that time-reversal \mathcal{T} is equivalent to a translation by $(\mathbf{a}_1 + \mathbf{a}_2 + \mathbf{a}_3)/2$ for these states, which leads to a twofold symmetry inside the unit cell reminiscent of anti-ferromagnetism.

In contrast, helical spin crystals with more than three modes like bcc, fcc, and \square depend essentially on the relative phases between the helical modes. For these states, \mathcal{T} is *not* equivalent to any translation, since it is not possible that $\exp(i\mathbf{k}_j \cdot \mathbf{a}) = -1$ for all \mathbf{k}_j . As a consequence, these states are doubly degenerate in addition to the translational degeneracy.

To obtain an understanding of the real-space picture of helical spin crystals, it is useful to study their symmetries under rotations (reflections change the chirality and therefore never appear in the symmetry group). For example, if the structure $\mathbf{M}(\mathbf{r})$ has a n -fold rotation axis with direction $\hat{\mathbf{u}}$, then $\mathbf{M} \parallel \hat{\mathbf{u}}$ along this axis. Therefore, \mathbf{M}_\perp , which is the projection to the plane orthogonal to $\hat{\mathbf{u}}$, has a node at the axis. The winding number²⁹ (vorticity) of the node is restricted by symmetry to the values $1, 1 \pm n, 1 \pm 2n$, etc. The resulting pattern in the vicinity of the rotation axis, \mathbf{M} pointing along $\hat{\mathbf{u}}$ in the center and \mathbf{M}_\perp winding around it, resembles that of a skyrmion or meron. Such patterns are currently being discussed in the context of helimagnets.^{21,22} Here, we observe that they naturally appear resulting from rotational symmetries. The simplest cases are winding numbers of $+1$ (for any n -fold axis) or -1 (only for $n=2$).

Apart from proper rotations, the point group may contain antirotations, i.e., symmetry operations which are composed of a rotation followed by \mathcal{T} . n -fold antirotation axes are only possible for even numbers n , since they imply $n/2$ -fold rotation symmetry. In the special case $n=2$, it merely follows that $\mathbf{M} \perp \hat{\mathbf{u}}$ along the axis, where $\hat{\mathbf{u}}$ is the axis direction. Higher antirotation symmetries with $n=4, 6, \dots$ imply $\mathbf{M}=0$ along the axis, i.e., they create a line node in the magnetization. In the vicinity of this line node, \mathbf{M} is approximately orthogonal to $\hat{\mathbf{u}}$ [as can be seen by expanding $\mathbf{M}(\mathbf{r})$ to linear order around a point on the axis]. The winding number of \mathbf{M}_\perp around the node, is restricted by symmetry to the values $1 \pm n/2, 1 \pm 3n/2, 1 \pm 5n/2$, etc. The simplest case for a fourfold antirotation axis is a winding number of -1 (antivortex line) and the simplest case for $n=6$ is a winding number of -2 .

We have thus demonstrated the emergence of topological objects like merons and antivortices, which are not expected to be stable in the present context of a vectorial order param-

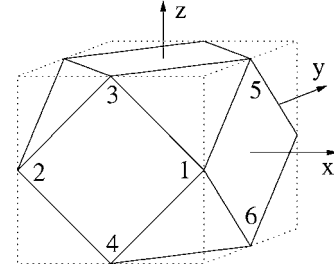


FIG. 5. Geometry of the wave vectors $\mathbf{k}_1, \dots, \mathbf{k}_6$, which constitute the bcc spin crystal states. The vectors $\pm\mathbf{k}_j$ form the vertices of a cuboctahedron.

eter in three dimensions but which are stabilized by symmetry. Thus, rotation axes are meron lines and fourfold antirotation axes are antivortex node lines.

1. Symmetry and real-space picture of bcc1

The bcc helical spin crystals consist of six helical modes with wave vectors $\hat{\mathbf{k}}_1 = [1\bar{1}0]$, $\hat{\mathbf{k}}_2 = [\bar{1}10]$, $\hat{\mathbf{k}}_3 = [0\bar{1}1]$, $\hat{\mathbf{k}}_4 = [01\bar{1}]$, $\hat{\mathbf{k}}_5 = [101]$, and $\hat{\mathbf{k}}_6 = [10\bar{1}]$, as shown in Fig. 5, and has the periodicity of a body-centered-cubic lattice. We choose the convention [see Eq. (4)]

$$\hat{\epsilon}_j'' = \frac{\hat{\mathbf{z}} \times \hat{\mathbf{k}}_j}{|\hat{\mathbf{z}} \times \hat{\mathbf{k}}_j|}, \quad (19)$$

for $j=1, \dots, 6$ with $\hat{\mathbf{z}} = [001]$, and we consider negative chirality [i.e., $\mathbf{M} \cdot (\nabla \times \mathbf{M}) < 0$], such that $\hat{\epsilon}_j' = \hat{\mathbf{k}}_j \times \hat{\epsilon}_j''$. The geometry of the wave vectors allows for three quartet terms in the free energy produced by $T_x = \psi_1^* \psi_2 \psi_5 \psi_6$, $T_y = \psi_1^* \psi_2^* \psi_3 \psi_4$, and $T_z = -\psi_3 \psi_4^* \psi_5^* \psi_6$. The sign in the definition of T_z has been introduced for convenience.

The transformation properties of the ψ variables and the three quartic terms under rotations are shown in Table I. From this, it can be deduced that the (rotation-invariant) quartet contribution to the free energy is

$$F_{\text{nt}} = 2\lambda_{\text{nt}} \text{Re}(T_x + T_y + T_z). \quad (20)$$

The value of the parameter λ_{nt} is not determined by symmetry. Direct calculation yields

$$\lambda_{\text{nt}} = \frac{7}{4} U \left[\frac{\pi}{3}, 2 \arccos\left(\frac{1}{3}\right) \right] - \frac{1}{2} U \left(\frac{\pi}{4}, \pi \right). \quad (21)$$

There are thus two bcc states, depending on the sign of λ_{nt} . In bcc1 (bcc2), which corresponds to $\lambda_{\text{nt}} > 0$ (< 0), the phases of the ψ 's are such that T_x, T_y, T_z are all negative (positive). Three out of the six phases are arbitrary due to global translation symmetry. This means that the magnetic pattern of bcc1 and bcc2 is uniquely determined up to translational and time-reversal degeneracy.

The solution for $\lambda_{\text{nt}} > 0$, bcc1, turns out to be the bcc structure with the highest point group symmetry. By selecting the coordinate origin conveniently, we obtain $-\psi_1 = \psi_2 = -i\psi_3 = i\psi_4 = i\psi_5 = -i\psi_6 = SM_0$ for bcc1, where $S = \pm 1$ is the time-reversal symmetry label and $M_0 > 0$ is the amplitude. From Table I, we deduce that $\mathbf{M}(\mathbf{r})$ changes sign under a

TABLE I. Transformation properties of the ψ variables and three quartic terms (defined in Sec. IV A 1) of the bcc spin crystals under rotations. R_z and R_x , respectively, are $\pi/2$ rotations around the z and x axis. These two rotations generate the cubic point group O and therefore, the behavior under any rotation which maps the 12 wave vectors onto each other may be obtained by combining these two operations.

	ψ'_1	ψ'_2	ψ'_3	ψ'_4	ψ'_5	ψ'_6	T'_x	T'_y	T'_z
R_z	ψ_2	ψ_1^*	ψ_6^*	ψ_5^*	ψ_3	ψ_4	T_y	T_x^*	T_z^*
R_x	$i\psi_5$	$-i\psi_6^*$	$-\psi_4^*$	ψ_3	$i\psi_2^*$	$i\psi_1$	T_x^*	T_z	T_y^*

$\pi/2$ rotation about the x , y or z axis. That is, the magnetic point group is $O(T)$ (international notation 432) with fourfold antirotation axes at $\langle 100 \rangle$, threefold rotation axes at $\langle 111 \rangle$, and twofold antirotation axes at $\langle 110 \rangle$.

The real-space representation of the bcc1 state is

$$\mathbf{M}(\mathbf{r}) = SM_0 \begin{pmatrix} \sqrt{2}s_x(c_y - c_z) - 2s_y s_z \\ \sqrt{2}s_y(c_z - c_x) - 2s_z s_x \\ \sqrt{2}s_z(c_x - c_y) - 2s_x s_y \end{pmatrix}, \quad (22)$$

where $s_x = \sin(Qx/\sqrt{2})$, $c_x = \cos(Qx/\sqrt{2})$, etc. The resulting pattern was shown in Fig. 2 of our earlier paper.²³ In Fig. 6, we show the symmetry axes. As discussed above, the magnetization must vanish along the fourfold antirotation axes, which are antivortices with winding number -1 . The x, y, z axes, and their translations according to the bcc periodicity, form two interpenetrating cubic lattices of such line nodes. The cubic space diagonals are threefold and the red arrowed lines of Fig. 6 are twofold rotation axes. In the vicinity of these lines, the magnetization field is skyrmionlike (i.e., \mathbf{M}_\perp has a winding number of $+1$).

The fact that the bcc1 state breaks T in a nontrivial way and cannot be restored by any translation is manifest in the occurrence of the T -breaking order parameter $\langle M_x M_y M_z \rangle = SM_0^3/2 \neq 0$, which is a magnetic octupole. This curious property may lead to distinctive anomalous effects, e.g., in the magnetotransport.³⁸ Octupolar magnetic ordering has recently been discussed in different contexts.³⁹

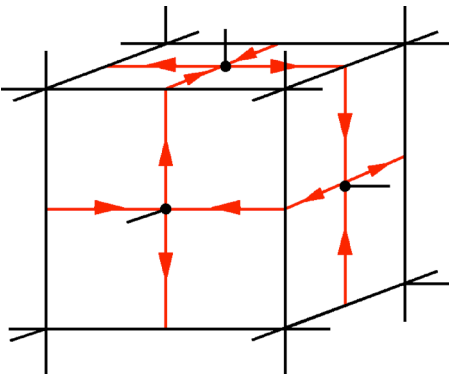


FIG. 6. (Color online). Symmetry of the bcc1 state. The figure shows a cubic unit cell of bcc1. Black lines are antivortex lines with fourfold antirotation symmetry and vanishing magnetization. The red (dark gray) lines are twofold rotation axes and the arrows indicate the direction of \mathbf{M} . The structure has threefold rotation symmetry about all cubic space diagonals.

2. Symmetry and real-space picture of sc

The simple-cubic (sc) helical spin crystal consists of three modes with $\hat{\mathbf{k}}_1 = [100]$, $\hat{\mathbf{k}}_2 = [010]$, and $\hat{\mathbf{k}}_3 = [001]$. It forms a periodic structure with a cubic unit cell and the lattice constant is $\lambda = 2\pi/Q$. The convention for ϵ'_j is given by Eq. (19), where the unit vector $\hat{\mathbf{z}}$ is replaced by $[111]$.

The transformation properties of the ψ variables under rotations are given in Table II. By choosing the center of coordinates corresponding to $\psi_1 = \psi_2 = \psi_3 = iM_0$, we obtain from Table II that the point group symmetry is $D_3(D_3)$ (international notation 32). That is, the chosen origin has a threefold rotation axis along $[111]$ and three twofold axes along $[1\bar{1}0]$, $[10\bar{1}]$, and $[01\bar{1}]$. Obviously, \mathbf{M} must vanish at a point of such high symmetry. Hence there is a point node at the origin.

Symmetry operations consisting of a rotation followed by an appropriate translation yield similar point nodes at $\frac{1}{2}\frac{3}{4}\frac{1}{4}$ (with threefold axis along $[\bar{1}11]$), $\frac{1}{4}\frac{1}{2}\frac{3}{4}$ (threefold axis $[1\bar{1}\bar{1}]$), and $\frac{3}{4}\frac{1}{4}\frac{1}{2}$ (threefold axis $[11\bar{1}]$). Finally, each of these nodes is doubled inside one unit cell because a translation by $(\frac{\lambda}{2}, \frac{\lambda}{2}, \frac{\lambda}{2})$ amounts to $\mathbf{M} \rightarrow -\mathbf{M}$. The twofold and threefold rotation axes form a complex array of skyrmionlike lines, all with winding numbers of $+1$. The real-space representation is

$$\mathbf{M}(\mathbf{r}) = SM_0 \begin{pmatrix} \tilde{c}_y - \tilde{s}_z \\ \tilde{c}_z - \tilde{s}_x \\ \tilde{c}_x - \tilde{s}_y \end{pmatrix}, \quad (23)$$

where $\tilde{s}_x = \sin[Q(x + \lambda/8)]$, $\tilde{c}_x = \cos[Q(x + \lambda/8)]$, etc.

B. Higher harmonics Fourier modes

As briefly mentioned in Sec. II B, magnetic ordering in wave vectors $\pm \mathbf{k}_j$ generally induces higher harmonics in the magnetic structure. In the presence of magnetic order $\mathbf{m}_{\mathbf{k}_j} \neq 0$, the Landau free energy for the modes $\mathbf{m}_{\mathbf{q}}$, which do not belong to the set $\mathbf{m}_{\mathbf{k}_j}$, is (to quartic order)

$$\Delta F = \sum_{\mathbf{q}} \tilde{r}_{\psi}(\mathbf{q}) |\mathbf{m}_{\mathbf{q}}|^2 - \mathbf{h}_{\psi}(\mathbf{q}) \cdot \mathbf{m}_{\mathbf{q}} - \mathbf{h}_{\psi}^*(\mathbf{q}) \cdot \mathbf{m}_{\mathbf{q}}, \quad (24)$$

with $\tilde{r}_{\psi}(\mathbf{q}) = r(q) + O(|\psi_j|^2)$ and

$$\mathbf{h}_{\psi}(\mathbf{q}) = -4 \sum'_{\mathbf{q}_1, \mathbf{q}_2, \mathbf{q}_3} U(\mathbf{q}_1, \mathbf{q}_2, \mathbf{q}_3) (\mathbf{m}_{\mathbf{q}_1} \cdot \mathbf{m}_{\mathbf{q}_2}) \mathbf{m}_{\mathbf{q}_3}, \quad (25)$$

where the sum is restricted to $\mathbf{q}_1, \mathbf{q}_2, \mathbf{q}_3 \in \{\pm \mathbf{k}_j\}$ such that $\mathbf{q}_1 + \mathbf{q}_2 + \mathbf{q}_3 = \mathbf{q}$. The origin of the exchange field \mathbf{h}_{ψ} is the

TABLE II. Transformation for the ψ variables of sc under rotations. R_z and R_x are $\pi/2$ rotations, $R_{[111]}$ is a $2\pi/3$ rotation, and $R_{[\bar{1}\bar{1}0]}$ is a π rotation around the indicated axis.

	R_x	R_y	R_z	$R_{[111]}$	$R_{[\bar{1}\bar{1}0]}$
ψ'_1	$i\psi_1$	$-i\psi_3$	ψ_2^*	ψ_3	$-\psi_2^*$
ψ'_2	ψ_3^*	$i\psi_2$	$-i\psi_1$	ψ_1	$-\psi_1^*$
ψ'_3	$-i\psi_2$	ψ_1^*	$i\psi_3$	ψ_2	$-\psi_3^*$

coupling term Eq. (5). In the following, we assume that $\bar{r}(\mathbf{q}) > 0$. Obviously, Eq. (24) then leads to induced modes

$$\mathbf{m}_{\mathbf{q}} = \frac{\mathbf{h}_{\psi, \mathbf{q}}}{\bar{r}(\mathbf{q})} \quad (26)$$

at momenta $\mathbf{q} = \pm \mathbf{k}_{j_1} \pm \mathbf{k}_{j_2} \pm \mathbf{k}_{j_3}$.⁴⁰ These modes modify the detailed magnetic structure, but they do not change its symmetry, since the field \mathbf{h}_{ψ} respects all the symmetries of the spin crystal.

We now briefly discuss the consequences for the three helical magnetic structures under consideration.

A single spin-density wave involving wave vectors $\pm \mathbf{k}$ might create higher harmonics at $\pm 3\mathbf{k}$ via Eq. (26). However, in the case of spin spirals, $\mathbf{m}_{\mathbf{k}} = 0$ and therefore $\mathbf{h}_{\psi, 3\mathbf{k}} = 0$. Thus, there are *no* higher harmonics created by a single spin spiral.

The sc spin structure with principal ordering wave vectors along $\langle 001 \rangle$ with $|\mathbf{k}_j| = Q$ generates higher harmonics along $\langle 111 \rangle$ (with $|\mathbf{q}| = \sqrt{3}Q$) and along $\langle 012 \rangle$ (with $|\mathbf{q}| = \sqrt{5}Q$). Note that throughout the current and last sections, all crystal directions refer to the magnetic crystals. The orientation of a magnetic crystal with respect to the atomic crystal depends on the anisotropy term F_a , which will be considered in Sec. V A 2.

In contrast to the former cases, bcc structures couple linearly to the $\mathbf{q} = 0$ mode (i.e., the uniform magnetization), since some triples of ordering vectors add to zero. This coupling will be further investigated in Sec. V B. Here, we only notice that for the bcc1 and bcc2 states, $\mathbf{h}_{\psi, \mathbf{q}=0} = 0$. This result can be understood in terms of the symmetry of these states. In the case of bcc1, the point group symmetry is too high to support a nonzero axial vector $\mathbf{h}_{\psi, \mathbf{q}=0}$. Therefore, bcc1 and bcc2 do not create a spontaneous net magnetization. The next set of wave vectors which can be reached by adding three ordering vectors are along $\langle 001 \rangle$ (with $|\mathbf{q}| = \sqrt{2}Q$). However for bcc1 and bcc2, direct calculation shows $\mathbf{h}_{\psi} = 0$ for these modes. As before, this can be understood in terms of symmetry. Higher harmonics along $\langle 001 \rangle$ would have the structure of a sc spin crystal. We have seen in Sec. III A, that the point group symmetry of sc is lower than that of bcc1. Therefore, bcc1 cannot create such an exchange field \mathbf{h}_{ψ} . We conclude that bcc1 creates *no* secondary Bragg peaks at $(0, 0, \sqrt{2}Q)$, etc. The same is true for bcc2. The shortest wave-vectors which are created by bcc1 or bcc2 as higher harmonics are along $\langle 112 \rangle$ (with $|\mathbf{q}| = \sqrt{3}Q$). Others are at $\langle 110 \rangle$ ($|\mathbf{q}| = 2Q$), $\langle 013 \rangle$ ($|\mathbf{q}| = \sqrt{5}Q$), $\langle 111 \rangle$ ($|\mathbf{q}| = \sqrt{6}Q$), and $\langle 123 \rangle$ ($|\mathbf{q}| = \sqrt{7}Q$).

V. RESPONSE TO CRYSTAL ANISOTROPY, MAGNETIC FIELD AND DISORDER

A. Effect of crystal anisotropy

So far, our free energy has been completely rotation invariant. In the magnetically ordered states, full rotation symmetry is spontaneously broken, but any global rotation of the spin structure leaves the energy invariant. This degeneracy is lifted by an additional anisotropy term F_a , which couples the magnetic crystal to the underlying atomic lattice. The crystal anisotropy energy is small and may be treated as a perturbation which merely selects the directional orientation, but does not otherwise affect the magnetic state.

1. Single-spiral state

In the case of a single-spiral state, crystal anisotropy is a function $F_a(\hat{\mathbf{k}})$, where $\hat{\mathbf{k}}$ is the spiral direction. The function $F_a(\hat{\mathbf{k}})$ may depend on various parameters, it should be symmetric under the point group of the (atomic) crystal lattice and satisfy $F_a(\hat{\mathbf{k}}) = F_a(-\hat{\mathbf{k}})$. For concreteness, we assume the cubic point group T , relevant for the B20 crystal structure. We further assume that $F_a(\hat{\mathbf{k}})$ is a slowly varying function, since a singular or rapidly oscillating function in reciprocal space would translate into a (nonlocal) interaction between magnetic moments and the atomic crystal. Such a function $F_a(\hat{\mathbf{k}})$ generally has its minimum at either $\langle 100 \rangle$ or $\langle 111 \rangle$, which can be shown in two different ways.

The first argument is based on combining symmetry with Morse's theory of critical points.⁴¹ Morse theory implies that

$$\text{maxima} - \text{saddles} + \text{minima} = 2 \quad (27)$$

for a function on the unit sphere. Symmetry requires that $F_a(\hat{\mathbf{k}})$ has stationary points (points with vanishing first derivative, i.e., maxima, minima or saddles) at $\langle 100 \rangle$ (six directions), $\langle 111 \rangle$ (eight directions), and $\langle 110 \rangle$ (12 directions). If $F_a(\hat{\mathbf{k}})$ is slowly varying, we suspect that these are the only stationary points, since adding more maxima, minima, and saddles means that the function is more rapidly oscillating. Under this hypothesis, it follows from Eq. (27), that the $\langle 110 \rangle$ directions are saddle points and that the extrema are at $\langle 111 \rangle$ and $\langle 100 \rangle$. For $\langle 110 \rangle$ to be minima, $F_a(\hat{\mathbf{k}})$ needs to have additional stationary points (e.g., saddles) at nonsymmetric, parameter-dependent locations. We conclude that an anisotropy which favors $\langle 110 \rangle$ would need to be more rapidly oscillating than required by symmetry.

The second argument is based on an expansion of $F_a(\hat{\mathbf{k}})$ in powers of the directions cosines $\hat{k}_x, \hat{k}_y, \hat{k}_z$:

TABLE III. Crystal directions of magnetic Bragg peaks and number of degenerate orientations for three magnetic structures, sc, bcc, and single-spiral, with crystal anisotropy given by Eq. (29).

	Spiral	No.	bcc	No.	sc	No.
$a > 0$	$\langle 111 \rangle$	4	$\langle 110 \rangle$	1	$\langle 122 \rangle$	4
$a < 0$	$\langle 100 \rangle$	3	$\langle 110 \rangle, \langle 114 \rangle^a$	4	$\langle 100 \rangle$	1

^aWhen averaged over domains, Bragg peaks along $\langle 110 \rangle$ are 2 times as intense as peaks along $\langle 114 \rangle$.

$$F_a(\hat{\mathbf{k}}) = \alpha(\hat{k}_x^4 + \hat{k}_y^4 + \hat{k}_z^4) + \alpha'(\hat{k}_x^2\hat{k}_y^2 + \hat{k}_y^2\hat{k}_z^2 + \hat{k}_z^2\hat{k}_x^2) + \dots, \quad (28)$$

where we retained the first two terms allowed by cubic symmetry. Because of the smallness of the wave vector sphere Q , one typically expects $|\alpha'| \ll |\alpha|$ and subsequent terms even smaller. It is easily checked that for most values of the parameters α, α' , Eq. (28) has its global minima at either $\langle 100 \rangle$ (for $\alpha < \min\{0, \alpha'/18\}$) or $\langle 100 \rangle$ (for $a > \max\{2\alpha'/9, \alpha'/18\}$). Only in the narrow parameter regime $0 < \alpha < 2\alpha'/9$, the minima are indeed at $\langle 110 \rangle$.⁴² We conclude that crystal anisotropy which favors $\langle 110 \rangle$ may only appear in a narrow regime between two phases which favor $\langle 111 \rangle$ and $\langle 100 \rangle$, respectively.

Accordingly, $\langle 111 \rangle$ or $\langle 100 \rangle$ are the selected spiral directions in all cubic helimagnets known so far.^{3,7,8} The preferred direction in MnSi at low pressure is $\langle 111 \rangle$ and in $\text{Fe}_x\text{Co}_{1-x}\text{Si}$, it is $\langle 100 \rangle$. In FeGe, there is a phase transition between these two directions,⁸ but no intermediate phase with $\langle 110 \rangle$ spiral orientation has been reported. However, the neutron scattering data¹⁵ in the partially ordered phase of MnSi clearly show a maximum signal along the $\langle 110 \rangle$ crystal directions. While it is initially tempting to interpret the partially ordered state of MnSi as a single-spiral state that has lost its orientational long-range order by some mechanism, one would still expect a maximal scattering intensity in the energetically preferred lattice direction. Theories of the partially ordered state in terms of disordered helical spin-density waves^{17,20} thus depend on a crystal anisotropy that prefers spiral directions along $\langle 110 \rangle$. As we have shown, this seems very unlikely.

2. Helical spin crystals

For multimode spin crystals, F_a is no longer determined by a single direction $\hat{\mathbf{k}}$, so the arguments of Sec. V A 1 do not apply. Rather, the anisotropy energy depends on three Euler angles, which rotate the full three-dimensional magnetic structure relatively to the atomic crystal. In other words, F_a is a function of the rotation group $\text{SO}(3)$. Relative to some standard orientation \mathbf{k}_j of the mode directions, the leading-order anisotropy term is

$$F_a(R) = a \sum_j g(R\hat{\mathbf{k}}_j) |\psi_j|^2, \quad (29)$$

where R is a rotation operator and $g(\hat{\mathbf{k}}) = \hat{k}_x^4 + \hat{k}_y^4 + \hat{k}_z^4$. As before, we have assumed a cubic point group symmetry.

In the case $a > 0$, the modes of the bcc spin crystals get locked to the $\langle 110 \rangle$ directions. The orientation of sc is four times degenerate if $a > 0$. The four minima of F_a are obtained from the standard orientation along $\langle 100 \rangle$ through a

$\pi/3$ rotation around any of the four space diagonals, such that the three spiral modes point along $\langle 122 \rangle$.

In the opposite case ($a < 0$), sc is oriented along $\langle 100 \rangle$. This time, it is the bcc spin crystals that get rotated by $\pi/3$ around any $\langle 111 \rangle$ axis to reach one of the four stable orientations. Under such $\pi/3$ rotations, three of the six modes remain along $\langle 110 \rangle$ and three move to $\langle 114 \rangle$. Each individual $\langle 114 \rangle$ direction appears only in one of the four solutions but each $\langle 110 \rangle$ direction appears in two of four solutions.

If there is more than one degenerate orientation, the sample typically breaks up into domains such that full cubic symmetry is restored in the neutron scattering signal. Table III lists the directions of magnetic Bragg peaks for the different cases. Out of the three prominent phases in our phase diagram, the bcc1 spin crystal is the only one that can explain the neutron-scattering peaks along $\langle 110 \rangle$ in the partial order phase of MnSi. It does so most naturally for the case $a > 0$, which is the known sign of the anisotropy in MnSi at low pressure.

In order to compare the energy scale of F_a (i.e., the locking energy) for the different magnetic states, we note the following. At the phase boundary between two equal-amplitude spin-crystal phases (one phase with amplitudes $|\psi_1| = \dots = |\psi_N|$ and the second phase with $|\tilde{\psi}_1| = \dots = |\tilde{\psi}_N|$) the amplitudes of the two neighboring phases are related by

$$N|\psi_j|^2 = \tilde{N}|\tilde{\psi}_{j'}|^2. \quad (30)$$

In the vicinity of the phase boundary, the anisotropy term is therefore proportional to the mode-average $1/N \sum_j g(R\hat{\mathbf{k}}_j)$. Using this result, we find that the effective anisotropy energy is smaller for the bcc spin crystals than for the single-spiral state by a factor of 4–4.5.⁴³ For the sc state, the locking energy is anisotropic. Certain rotations are equally costly in energy as for the single-spiral case while some small rotations about the minimum for $a > 0$ are softer than for the single spiral by a factor of 4.5.

B. Effect of magnetic field

A uniform external magnetic field \mathbf{H} couples to the $\mathbf{q}=0$ mode of the magnetization, $\mathbf{m} = \langle \mathbf{M} \rangle$, via Zeeman coupling. The uniform magnetization, in turn, couples to the helical modes ψ_j through

$$F = F|_{\mathbf{m}=0} + r_0 \mathbf{m}^2 + U(0,0,0) \mathbf{m}^4 - \mathbf{h}_{\psi}(0) \mathbf{m} + 2 \sum_j (U(\mathbf{k}_j, -\mathbf{k}_j, 0) \mathbf{m}^2 + U(\mathbf{k}_j, 0, 0) \mathbf{m}_{\perp,j}^2) |\psi_j|^2, \quad (31)$$

where $\mathbf{m}_{\perp,j} = \mathbf{m} - (\mathbf{m} \cdot \hat{\mathbf{k}}_j) \hat{\mathbf{k}}_j$ and we have used Eqs. (5) and

(25). Plumer and Walker⁴⁴ argued that $U(0,0,0) \approx U(\mathbf{k}_j, -\mathbf{k}_j, 0) \approx U_s$, which we will use in the following for simplicity.

1. Response of the single-spiral state

The behavior of the single-mode spiral state under a magnetic field has been studied both experimentally^{3,8-10,12} and theoretically.^{45,44} It is characterized by a strongly anisotropic susceptibility, induced by the last term in Eq. (31). For a fixed spiral direction \mathbf{k} , the susceptibilities parallel and orthogonal to the spiral direction are given by

$$\chi_{\parallel} \approx \Delta^{-1},$$

$$\chi_{\perp} \approx \left(\Delta + 2 \frac{U'}{U_s} |r(Q)| \right)^{-1}, \quad (32)$$

where $\Delta = 2[r_0 - r(Q)] = 2JQ^2$ and $U' = U(\mathbf{k}, 0, 0)$. Well below the critical ordering temperature, $\Delta \ll 2|r(Q)|$ and therefore $\chi_{\parallel} \gg \chi_{\perp}$. This strong anisotropy leads to a spin reorientation transition at $H = H_{\text{sr}}$, where the spiral axis gets oriented along the field direction. The value of H_{sr} depends on the anisotropy [Eq. (28)] and the field direction. For $\alpha > 0$ and $\mathbf{H} \parallel \langle 100 \rangle$, Plumer and Walker obtained

$$H_{\text{sr}}^2 = \frac{4\alpha}{\chi_{\parallel} - \chi_{\perp}} \gtrsim 4\alpha\Delta, \quad (33)$$

where we have used $\chi_{\parallel} \gg \chi_{\perp} > 0$. Once the spiral is oriented, the susceptibility is large (equal to χ_{\parallel}).

The spiral amplitude decreases as a function of the external field and vanishes at

$$H_c = |\psi_0| \Delta, \quad (34)$$

where $|\psi_0|^2 = |r(Q)| / (2U_s)$. Above H_c , the magnetization is uniform.

2. Response of the bcc1 spin crystal

In the bcc spin crystal states, the linear response is isotropic, because their symmetry group does not allow for an anisotropic susceptibility tensor. As a consequence, there is no orientation of the bcc state towards the magnetic field at the level of linear response (i.e., from energies up to order \mathbf{H}^2). However, there is a subleading contribution to the energy $\propto \langle M_x M_y M_z \rangle H_x H_y H_z$. This contribution splits the degeneracy between the $S=1$ and $S=-1$ states and it may lead to a reorientation of the bcc crystal towards the field.

In terms of the six ψ variables of bcc, the exchange field $\mathbf{h}_{\psi}(0)$, which enters Eq. (31), amounts to

$$\mathbf{h}_{\psi}(0) = -\mu \text{Re}[(5 - \sqrt{2}i)\tilde{\mathbf{h}}_{\psi}], \quad (35)$$

where $\mu = U(\mathbf{k}_{j_1}, \mathbf{k}_{j_2}, \mathbf{k}_{j_3})$ for $\mathbf{k}_{j_1} + \mathbf{k}_{j_2} + \mathbf{k}_{j_3} = 0$ and

$$\tilde{\mathbf{h}}_{\psi} = \psi_1 \psi_3^* \psi_6^* \begin{pmatrix} 1 \\ 1 \\ 1 \end{pmatrix} + \psi_1^* \psi_4 \psi_5 \begin{pmatrix} -1 \\ -1 \\ 1 \end{pmatrix} - \psi_2 \psi_4^* \psi_6 \begin{pmatrix} -1 \\ 1 \\ -1 \end{pmatrix} - \psi_2^* \psi_3 \psi_5^* \begin{pmatrix} 1 \\ -1 \\ -1 \end{pmatrix}. \quad (36)$$

The (isotropic) inverse spin susceptibility (see the Appendix) in the bcc1 state is composed of three contributions

$$\chi_{\text{bcc1}}^{-1} = \chi_{\text{bare}}^{-1} + \chi_{\text{phase}}^{-1} + \chi_{\text{amp}}^{-1}. \quad (37)$$

The first term

$$\chi_{\text{bare}}^{-1} = 2 \left(r_0 + \frac{U_s + \frac{2}{3}U'}{U_{\text{bcc1}}} |r(Q)| \right), \quad (38)$$

where $U_{\text{bcc1}} = 1/6[U_s + V_p(\pi/4) + 4V_p(\pi/6) - \lambda_{\text{nt}}]$, can be derived in analogy to the single-spiral case. In fact, χ_{bare} is a ‘‘mixture’’ of χ_{\parallel} and χ_{\perp} , determined geometrically by the angles between the mode directions \mathbf{k}_j and the magnetic field. It follows that $\chi_{\text{bare}} \leq \chi_{\parallel}$, provided $U_{\text{bcc1}} \sim U_s$ (the two couplings are equal at the phase boundary between single spiral and bcc1). The remaining terms in Eq. (37),

$$\chi_{\text{phase}}^{-1} = -\frac{\mu^2 |r(Q)|}{3U_{\text{bcc1}} \lambda_{\text{nt}}},$$

$$\chi_{\text{amp}}^{-1} = -\frac{25\mu^2 |r(Q)|}{12U_{\text{bcc1}} [U_s - V_p(\pi/4) + \lambda_{\text{nt}}]}, \quad (39)$$

stem from the response of the bcc magnetic structure to the field. That is, they originate from the adjustments of relative phases and amplitudes, respectively, of the helical modes as a result of the term $-\mathbf{h}_{\psi}(0) \cdot \mathbf{m}$ in Eq. (31). The effect of χ_{phase} and χ_{amp} , which are necessarily negative, is to increase the susceptibility of the bcc1 state.

The change in the relative amplitudes and phases of the six interfering spirals as a function of the magnetic field may be calculated (see the Appendix). For example, the linear response of the amplitudes of bcc1 is

$$\begin{pmatrix} \delta|\psi_1| \\ \delta|\psi_2| \\ \delta|\psi_3| \\ \delta|\psi_4| \\ \delta|\psi_5| \\ \delta|\psi_6| \end{pmatrix} = \frac{5\mu S}{4[U_s - V_p(\pi/4) + \lambda_{\text{nt}}]} \begin{pmatrix} -m_z \\ m_z \\ -m_x \\ m_x \\ m_y \\ -m_y \end{pmatrix}. \quad (40)$$

This response should be observable by neutron scattering, if it is possible to prepare the sample in a single-domain state (i.e., without mixture of the two time-reversal partners). For example, a field in $\hat{\mathbf{z}}$ direction affects $|\psi_1|$ and $|\psi_2|$, the amplitudes of the modes propagating orthogonally to $\hat{\mathbf{z}}$ (Fig. 5), which get enhanced and suppressed by the magnetic field, respectively.

The expected effects of external magnetic field on the resistivity of bcc spin crystal are presented elsewhere.³⁸

VI. EFFECT OF IMPURITIES: A POSSIBLE ROUTE TO PARTIAL ORDER

While the helical spin crystal states are expected to show Bragg spots at particular wave vectors, a variety of effects such as thermal or quantum fluctuations or disorder can destroy the long range order while preserving the helical spin crystal structure at shorter scales. Here, we investigate in more detail the effect of nonmagnetic disorder on helical spin crystal structures.

Although the experimentally studied helimagnets are very clean from the electrical resistivity point of view, the helical magnetic structures are sensitive to disorder at a much longer length scale. In addition, the low energy scales required to distort them means that one needs to consider disorder effects. An observation that can immediately be made is that for the physically relevant case of nonmagnetic disorder [$V_{\text{dis}}(\mathbf{r})$], the single-spiral state and the spin crystal states respond very differently. By symmetry, the coupling of disorder to the magnetic structure is given by $F_{\text{dis}} = \langle V_{\text{dis}}(\mathbf{r})|\mathbf{M}(\mathbf{r})|^2 \rangle$. Hence, single-spiral states which are unique in having a spatially uniform magnitude of magnetization [$|\mathbf{M}(\mathbf{r})| = \text{constant}$] are unaffected by this coupling; in contrast the spin-crystal states necessarily have a modulated magnitude²³ and hence are affected by nonmagnetic disorder. Therefore the neutron scattering signal of the spin-crystal state is expected to have more diffuse scattering than the single mode state. This is consistent with the experimental observation that the high pressure phase has diffuse scattering peaked about $\langle 110 \rangle$ while the low pressure phase has sharper spots, consistent with identifying the two as spin-crystal and single-spiral states, respectively.

The effect of disorder on the spin-crystal state is closely related to the problem of the ordering of an XY model in the presence of a random external field. The phase rotation symmetry of the XY model captures the translational invariance of the spin crystal in the clean state. Disorder destroys this invariance and behaves like a random field applied to the XY system. Using the insights from the study of that problem in three dimensions,⁴⁶ one expects that for weak disorder a Bragg glass will result, where although true long range order is destroyed, power law divergent peaks at the Bragg wave vectors remain, and the elastic constants remain finite. For stronger disorder one expects this algebraic phase to also be destroyed, and recover a short range correlated phase without elasticity. Nevertheless, for the case of the bcc1 and bcc2 crystals, due to time reversal symmetry (\mathcal{T}) breaking in these states, the disordered states also spontaneously break time-reversal symmetry, and hence a phase transition is expected on cooling despite the absence of long range order. It is difficult to predict which of these two scenarios (Bragg glass or only \mathcal{T} breaking) is more appropriate for MnSi. In the latter case one may estimate the spreading of the Bragg spots due to disorder by considering the energetic cost to deform the spin-crystal state in different ways.

Ignoring elastic contributions, there are two distinct types of deformations—ones that involve a change in the magnitude of the ordering wave vectors δq_{\parallel} and others that do not change the wave vector magnitude but rotate the structure

from its preferred orientation, δq_{\perp} . The second is expected to be low in energy because rotations of the structure are locked by the crystal anisotropy term, which is weak. From Eq. (28), we obtain the energy cost to shift the ordering vector by δq_{\perp} along the sphere $|\mathbf{q}|=Q$,

$$\delta F_{\perp} = \frac{4\alpha}{3\kappa} \left(\frac{\delta q_{\perp}}{Q} \right)^2, \quad (41)$$

where $\kappa=1$ for the single spiral. For multimode spin crystals, the energy cost of rotation is reduced, as explained in Sec. V A 2. Thus, $\kappa \approx 4$ for the bcc spin crystals. In contrast, deformations that change the magnitude of the ordering wave vectors, must contend with the DM interaction scale, and hence pay a higher energy penalty

$$\delta F_{\parallel} = \frac{1}{2} \Delta |\psi_0|^2 \left(\frac{\delta q_{\parallel}}{Q} \right)^2. \quad (42)$$

Assuming the disorder couples to these deformations equally, we can estimate the ratio of their amplitudes in the limit of weak deformations, by equating Eqs. (41) and (42). It follows

$$\left(\frac{\delta q_{\perp}}{\delta q_{\parallel}} \right)^2 = \frac{3\kappa\Delta |\psi_0|^2}{8\alpha}. \quad (43)$$

Using Eqs. (33) and (34), we can relate this ratio to the experimentally known ratio between the critical magnetic fields for, respectively, reorienting and polarizing the single-spiral state

$$\frac{\delta q_{\perp}}{\delta q_{\parallel}} \gtrsim \sqrt{\frac{3\kappa H_c}{2 H_{\text{sr}}}}. \quad (44)$$

We can now apply these results to the case of MnSi and test the hypothesis that the partial order state is in fact a disordered bcc spin crystal. Setting in $\kappa=4$ and the experimentally measured¹² critical fields for MnSi, $H_c=0.6$ Tesla and $H_{c1}=0.1$ Tesla, one obtains $\delta q_{\perp}/\delta q_{\parallel} \gtrsim 15$. Neutron scattering experiments do indeed find that the transverse broadening is larger than the longitudinal broadening, but since the latter is resolution limited, this only gives us a lower bound that is consistent with the estimate above $(\delta q_{\perp}/\delta q_{\parallel})_{\text{expt}} > 2.3$. Nevertheless, the trend that the width of the spot is greater along the equal magnitude sphere than transverse to it is clearly seen in the experimental data.

Thus, weak nonmagnetic disorder of the atomic crystal is expected to destroy magnetic long range order in multimode helical spin crystal states and lead to a neutron scattering signal compatible with the observations in the partial order phase of MnSi. However in the case of bcc spin crystals, time-reversal symmetry breaking is expected to persist even in the presence of disorder. The scenario of interpreting partial order in MnSi as a bcc1 state disordered by impurities thus predicts quasistatic local magnetic moments and implies a finite temperature phase transition on cooling into this phase.

VII. CONCLUSION

We have analyzed the magnetic properties of noncentrosymmetric weak ferromagnets subject to DM spin-orbit coupling. This problem falls into the general class of systems where the low energy excitations live on a surface in reciprocal space rather than on discrete points. The addition of DM interactions to a ferromagnetic state produces a large degeneracy of magnetic states characterized by arbitrary superpositions of spin helices of a fixed helicity and fixed wave vector magnitude. This enormous degeneracy is broken by interactions between modes, and the single-spiral state is realized for slowly varying interactions, by virtue of its unique property of having a spatially uniform magnitude of magnetization. For more general interactions, multimode helical spin crystal states are obtained. We show that for the model interactions considered, the phase diagram is largely determined just by considering the interactions between pairs of modes. The phase that is eventually realized may be readily deduced from the range of angles in which this interaction drops below a critical value. In particular, the bcc structure is stabilized by virtue of the fact that its reciprocal lattice, fcc, is a close packed structure. These results may also be relevant in other physical situations where crystallization occurs, such as the Larkin-Ovchinnikov-Fulde-Ferrel instability in spin-imbalanced superconductors, which may potentially be realized in solid state systems,⁴⁷ cold atomic gases,⁴⁸ and dense nuclear matter.⁴⁹

Helical spin crystals typically give rise to complicated real space magnetic structures which we discussed in this paper. In particular, topological textures like merons and antivortices can be seen about special axes in particular realizations, although these are not expected to be stable given the order parameter and spatial dimensionality of the system. We show here that such topological structures exist as a consequence of symmetry, which also dictates the absence of certain higher Bragg reflections, which a naive analysis would predict.

The response of helical spin crystals to crystalline anisotropy and applied magnetic field are considered with a special emphasis on the bcc structures which are contrasted against the response of the single helix state. An unusual transfer of spectral intensity in the presence of an applied magnetic field, which is strongly dependent on the direction of applied field is noted for the bcc structures. This is a consequence of broken time-reversal symmetry in the absence of a net magnetization (which is symmetry forbidden). The unusual magnetotransport in such a state, a linear in field magnetoresistance and quadratic Hall effect, has been discussed briefly in Ref. 23 and was elaborated upon in Ref. 38.

Helical spin crystals exhibit Bragg peaks at specific wave vectors, and hence are not directly consistent with the experimental observation of partial order. The point of view taken in our earlier work²³ is that the short distance and short time properties are captured by the appropriate helical spin crystal structure. Studying the properties of helical spin crystals with

long range order is a theoretically well-defined task with direct consequences for a proximate disordered phase with similar correlations up to some intermediate scale. The mechanism that leads to the destruction of long range helical spin crystal order is unclear; in Ref. 23, this was assumed to be the coupling to nonmagnetic disorder. Then, as elaborated in this paper, beginning with a bcc helical spin crystal a neutron scattering signature consistent with that of partial order may be obtained. However, within the simplest version of this scenario, one also expects a finite temperature phase transition where time-reversal symmetry breaking develops, and static magnetic order which may be seen in nuclear magnetic resonance or muon spin rotation experiments. Other mechanism for the destruction of long range order of the bcc spin-crystal state, such as thermal or quantum fluctuations may also be considered, but are left for future work.

ACKNOWLEDGMENTS

The authors would like to thank L. Balents, P. Fazekas, I. Fischer, D. Huse, J. Moore, N. Nagaosa, M.P. Ong, C. Pfleiderer, D. Podolsky, A. Rosch, T. Senthil, H. Tsunetsugu, and C. Varma for useful and stimulating discussions and V. Aji for an earlier collaboration on related topics. This work was supported by the Swiss National Science Foundation, the A.P. Sloan Foundation, and Grant No. DE-AC02-05CH11231.

APPENDIX: LINEAR RESPONSE

Let the free energy F depend on real internal variables $\mathbf{x}=(x_1, \dots, x_n)$ (related to various order parameters) and on $\mathbf{m}=(m_1, m_2, m_3)$, which couples linearly to the external field \mathbf{H} . The internal variables are chosen such that for $\mathbf{m}=0$, the minimum energy shall be at $\mathbf{x}=0$. Expanding F to second order in \mathbf{x} and \mathbf{m} yields

$$F = \frac{1}{2} \mathbf{x}^T A \mathbf{x} + \mathbf{m}^T B \mathbf{x} + \frac{1}{2} \mathbf{m}^T C \mathbf{m}, \quad (\text{A1})$$

where A , B , and C are matrices, $A=A^T$, $C=C^T$. All eigenvalues of A are positive. Equation (A1) can be written as

$$F = \frac{1}{2} (\mathbf{x} - \mathbf{x}_m)^T A (\mathbf{x} - \mathbf{x}_m) + \frac{1}{2} \mathbf{m}^T \chi^{-1} \mathbf{m}, \quad (\text{A2})$$

where $\mathbf{x}_m = -A^{-1} B^T \mathbf{m}$ and $\chi^{-1} = C - B A^{-1} B^T$. It follows that under the influence of an external field \mathbf{H} , the equilibrium internal variables get shifted to $\mathbf{x} = \mathbf{x}_m$ and the linear response is given by $\mathbf{m} = \chi \mathbf{H}$. Thus, there are two contributions to the inverse susceptibility: $\chi_{\text{bare}}^{-1} = C$ and $\chi_x^{-1} = -B A^{-1} B^T$. The latter comes from the internal response of the x variables to the magnetic field.

These general results are applied in Sec. V B 2, where the internal variables x_1, \dots, x_9 are the deviations from their equilibrium value at $\mathbf{m}=0$ of six amplitudes $|\psi_j|$ and three phases (holding the other three phases fixed). In this case, χ_x leads to both the phase and amplitude related terms in Eq. (39).

*Electronic address: binzb@thp.uni-koeln.de

- ¹I. Dzyaloshinskii, J. Phys. Chem. Solids **4**, 241 (1958); T. Moriya, Phys. Rev. **120**, 91 (1960).
- ²I. Dzyaloshinskii, Zh. Eksp. Teor. Fiz. **46**, 1420 (1964); **47**, 336 (1964); **47**, 992 (1964) [Sov. Phys. JETP **19**, 960 (1964); **20**, 223 (1965); **20**, 665 (1965)].
- ³Y. Ishikawa, K. Tajima, D. Bloch, and M. Roth, Solid State Commun. **19**, 525 (1976).
- ⁴T. Moriya, Solid State Commun. **20**, 291 (1976); K. Makoshi and T. Moriya, J. Phys. Soc. Jpn. **44**, 80 (1978).
- ⁵O. Nakanishi, A. Yanase, A. Hasegawa, and M. Kataoka, Solid State Commun. **35**, 995 (1980).
- ⁶P. Bak and M. H. Jensen, J. Phys. C **13**, L881 (1980).
- ⁷J. Beille, J. Voiron, and M. Roth, Solid State Commun. **47**, 399 (1983).
- ⁸B. Lebech, J. Bernhard, and T. Freltoft, J. Phys.: Condens. Matter **1**, 6105 (1989).
- ⁹K. Ishimoto, Y. Yamaguchi, J. Suzuki, M. Arai, M. Furusaka, and Y. Endoh, Physica B **213-214**, 381 (1995).
- ¹⁰M. Uchida, Y. Onose, Y. Matsui, and Y. Tokura, Science **311**, 359 (2006).
- ¹¹C. Pfleiderer, G. J. McMullan, S. R. Julian, and G. G. Lonzarich, Phys. Rev. B **55**, 8330 (1997).
- ¹²C. Thessieu, C. Pfleiderer, A. N. Stephanov, and J. Flouquet, J. Phys.: Condens. Matter **9**, 6677 (1997).
- ¹³C. Pfleiderer, S. R. Julian, and G. G. Lonzarich, Nature (London) **414**, 427 (2001); N. Doiron-Leyraud, I. R. Walker, L. Taillefer, M. J. Steiner, S. R. Julian, and G. G. Lonzarich, *ibid.* **425**, 595 (2003).
- ¹⁴W. Yu, F. Zamborszky, J. D. Thomson, J. L. Sarrao, M. E. Torelli, Z. Fisk, and S. E. Brown, Phys. Rev. Lett. **92**, 086403 (2004).
- ¹⁵C. Pfleiderer, D. Reznik, L. Pintschovius, H. v. Löhneysen, M. Garst, and A. Rosch, Nature (London) **427**, 227 (2004).
- ¹⁶I. Fischer and A. Rosch, Europhys. Lett. **68**, 93 (2004).
- ¹⁷S. V. Grigoriev, S. V. Maleyev, A. I. Okorokov, Y. O. Chetverikov, R. Georgii, P. Böni, D. Lamago, H. Eckerlebe, and K. Pranzas, Phys. Rev. B **72**, 134420 (2005); S. V. Maleyev, *ibid.* **73**, 174402 (2006).
- ¹⁸D. Belitz, T. R. Kirkpatrick, and A. Rosch, Phys. Rev. B **73**, 054431 (2006); **74**, 024409 (2006).
- ¹⁹J. Schmalian and M. Turlakov, Phys. Rev. Lett. **93**, 036405 (2004).
- ²⁰S. Tewari, D. Belitz, and T. R. Kirkpatrick, Phys. Rev. Lett. **96**, 047207 (2006).
- ²¹U. N. Bogdanov, U. K. Rössler, and C. Pfleiderer, Physica B **359-361**, 1162 (2005); U. K. Rössler, U. N. Bogdanov, and C. Pfleiderer, Nature (London) **442**, 797 (2006).
- ²²I. Fischer and A. Rosch (private communication).
- ²³B. Binz, A. Vishwanath, and V. Aji, Phys. Rev. Lett. **96**, 207202 (2006).
- ²⁴D. Mukamel and S. Krinsky, Phys. Rev. B **13**, 5065 (1976).
- ²⁵T. Jo, J. Phys. F: Met. Phys. **13**, L211 (1983).
- ²⁶E. M. Forgan, E. P. Gibbons, K. A. McEwen, and D. Fort, Phys. Rev. Lett. **62**, 470 (1989).
- ²⁷M. J. Longfield, J. A. Paixão, N. Bernhoeft, and G. H. Lander, Phys. Rev. B **66**, 054417 (2002).
- ²⁸J. R. Stewart, G. Ehlers, A. S. Wills, St. T. Bramwell, and J. S. Gardner, J. Phys.: Condens. Matter **16**, L321 (2004).
- ²⁹N. D. Mermin, Rev. Mod. Phys. **51**, 591 (1979).
- ³⁰S. A. Brazovskii, I. E. Dzyaloshinskii, and A. R. Muratov, Sov. Phys. JETP **66**, 625 (1988) [Zh. Eksp. Teor. Fiz. **93**, 1110 (1987)].
- ³¹Effective interaction vertices of interacting electrons are known to develop singular momentum-dependence close to Fermi liquid instabilities. See, for example, B. Binz, D. Baeriswyl, and B. Douçot, Eur. Phys. J. B **25**, 69 (2002).
- ³²A. Vishwanath and B. Binz (unpublished).
- ³³Whenever $W' < 0$, Eq. (16) becomes negative for a rapidly varying M^2 and the quartic theory is thus unstable. We consciously ignore this instability, since we only study local minima at small M^2 , where F_2 is dominant and forbids rapid variations.
- ³⁴Only the relative orientation between these modes enters the calculation, not their orientation with respect to the atomic lattice, since crystal anisotropy is neglected.
- ³⁵To obtain the phase diagram of Figs. 2 and 3, we have used the approximation $(1+x)^{5/2} + (1-x)^{5/2} \approx 2 + (4\sqrt{2}-2)x^2$ for $x = \cos \theta$ in the evaluation of $V_p(\theta)$. The error is smaller than 0.7%.
- ³⁶The shift to directions $(\pm\sqrt{1+\delta} \pm \sqrt{1+\delta}\sqrt{1-2\delta})$ is very small with $\delta \sim 0.02$ and even without the deformation, fcc would still beat the neighboring phases in the fcc* region.
- ³⁷Without having a rigorous proof, we suspect that in the context of Sec. III C, “very big” just means “bigger than U_s .” This bound has proven sufficient in all cases that we have tested.
- ³⁸B. Binz and A. Vishwanath, J. Magn. Magn. Mater. (to be published).
- ³⁹R. Caciuffo, J. A. Paixão, C. Detlefs, M. J. Longfield, P. Santini, N. Bernhoeft, J. Rebizant, and G. H. Lander, J. Phys.: Condens. Matter **15**, S2287 (2003); A. Kiss and P. Fazekas, Phys. Rev. B **68**, 174425 (2003).
- ⁴⁰In nonmagnetic crystals, the coupling term is cubic and therefore higher harmonics are generated at all sums of *two* momenta $\mathbf{k}_{j1} \pm \mathbf{k}_{j2}$. In magnetic structures, higher-harmonics wave vectors are restricted to sums of *three* ordering momenta.
- ⁴¹M. Morse, *The Calculus of Variations in the Large* (American Mathematical Society, Providence, RI, 1934), Vol. 18.
- ⁴²In this regime, all 26 high-symmetry points are extrema of F_a and 24 saddle points are located at $\langle \sqrt{2}\alpha\sqrt{2\alpha}\sqrt{\alpha'-4\alpha} \rangle$, in agreement with Eq. (27).
- ⁴³Using $\max\{F_a\} - \min\{F_a\}$ to estimate the locking energy scale leads to a reduction factor of 4.5. Expanding F_a around its minimum for $a > 0$ leads to a factor of 4.
- ⁴⁴M. L. Plumer and M. B. Walker, J. Phys. C **14**, 4689 (1981).
- ⁴⁵M. Kataoka and O. Nakanishi, J. Phys. Soc. Jpn. **50**, 3888 (1981).
- ⁴⁶T. Giamarchi and P. Le Doussal, Phys. Rev. B **52**, 1242 (1995).
- ⁴⁷H. A. Radovan *et al.*, Nature (London) **425**, 6953 (2003); K. Kakuyanagi, M. Saitoh, K. Kumagai, S. Takashima, M. Nohara, H. Takagi, and Y. Matsuda, Phys. Rev. Lett. **94**, 047602 (2005).
- ⁴⁸M. W. Zwierlein, A. Schirotzek, C. H. Schunck, and W. Ketterle, Science **311**, 492 (2006); G. B. Partridge, W. Li, R. I. Kamar, Y. Liao, and R. G. Hulet, *ibid.* **311**, 503 (2006).
- ⁴⁹J. A. Bowers and K. Rajagopal, Phys. Rev. D **66**, 065002 (2002).